Extremely Strong Near-IR Two-Photon Absorption in Conjugated Porphyrin Dimers: Quantitative Description with Three-Essential-States Model

Mikhail Drobizhev,[†,‡] Yuriy Stepanenko,[†,§] Yuliya Dzenis,[†] Aliaksandr Karotki,[†] Aleksander Rebane,*,[†] Peter N. Taylor,[||] and Harry L. Anderson[||]

Department of Physics, Montana State University, Bozeman, Montana 59717, P. N. Lebedev Physics Institute, Leninsky Pr., 53, 119991 Moscow, Russia, Institute of Physical Chemistry, Polish Academy of Sciences, Kasprzaka 44/52, 01-224 Warsaw, Poland, and Department of Chemistry, Chemistry Research Laboratory, University of Oxford, Mansfield Road, Oxford OX1 3TA, United Kingdom

Received: December 16, 2004; In Final Form: February 11, 2005

Two-photon absorption spectra (2PA) of a series of conjugated dimers and the corresponding monomer were studied in the near-IR region. All of the dimers show very large peak cross section values, $\sigma_2 = (3-10) \times 10^3$ GM (1 GM = 1×10^{-50} cm^4 s photon^{-1}), which is several hundred times larger than that obtained for the corresponding monomer in the same region. We explain such dramatic cooperative enhancement by a combination of several factors, such as strong enhancement of the lowest one-photon Q-transition, better resonance conditions in the three-level system, dramatic enhancement of the excited-state singlet−singlet transition, and parallel arrangement of consecutive transitions in dimers, as compared to perpendicular arrangement in the monomer. We show that the absolute values of the 2PA cross section in these molecules are quantitatively described by a quantum-mechanical expression, derived for the three-level model. We also demonstrate the possibility of singlet oxygen generation upon one- and two-photon excitation of these dimers, which makes them particularly attractive for photodynamic therapy.

1. Introduction

Chromophores capable of highly efficient two-photon absorption (2PA) are extremely needed for several innovative applications, such as fluorescence three-dimensional (3D) microscopy,[1] deeper-penetrating photodynamic therapy of cancer (PDT),[2] 3D micro- and nanofabrication,[3] high-density optical data storage,[4] and others. Porphyrins and other tetrapyrrolic compounds deserve particular attention in this connection, first because they have been commonly accepted for decades as tumor markers and photosensitizers in PDT[5] and also because they can participate in various photochemical processes that are promising for optical memory[6] and microfabrication. However, the 2PA properties of tetrapyrroles were almost ignored until recently. In those few cases where 2PA cross section values, σ_2, were measured, they were rather small, 1−10 GM (1 GM = 1×10^{-50} cm^4 s photon^{-1}).[7]

In a series of papers,[8] we have started a detailed study of the 2PA spectra and absolute cross sections of a vast series of tetrapyrrolic compounds and have established several of their special 2PA features. First, we have found that the effect of resonance enhancement of 2PA, which occurs if the excitation wavelength is tuned close to the one-photon-allowed Q-transition, is rather general for most tetrapyrroles.[8c−e] Second, in the region of one-photon Soret transition of some substituted tetraazoporphyrins, we have detected strong two-photon allowed peaks, corresponding to gerade excited states.[8d] Furthermore,

by means of symmetrical[8d] or asymmetrical[8h] chemical modification of the bare tetrapyrroles, we were able to drastically increase the 2PA cross section in the near-IR region, up to $\sigma_2 \approx 10^3$ GM. These values are comparable to those of the strongest organic 2PA chromophores.[9]

Recently, we have also found[8g] that a *meso*-butadiyne-linked symmetrical porphyrin dimer, yPyyPy (Figure 1), possesses an extremely large intrinsic (femtosecond) two-photon absorption cross section in the near-IR region, amounting to $\sigma_2 = 6 \times 10^3$ GM at the excitation wavelength $\lambda_{exc} = 780$ nm. This corresponds to a factor of ~*400* of enhancement in the dimer as compared to the parent monomer, yPy, measured at the same wavelength. We have shown[8g] that only a certain part of this enhancement (13 times) is due to the closer distance between the lowest Q-transition and the excitation wavelength. The remaining factor of 30 was assumed to be due to a very advantageous combination of inherent molecular properties of the dimer.

2PA cross sections of other butadiyne-linked bisporphyrin dimers were also recently measured with the femtosecond open-aperture *z*-scan method in the near-IR region giving values of a few thousand GM.[10] Furthermore, degenerate four wave mixing (DFWM) studies on a polymer analogue of the above yPyyPy dimer indicate that it may have a cross section as high as 5×10^4 GM per macrocycle at the excitation wavelength of 1064 nm.[11]

To better understand the nature of this strong enhancement effect in conjugated porphyrin polymer systems and elucidate the role of molecular structure, we present here a comprehensive study[12] of one-photon and two-photon spectra of a series of dimers with different π-conjugated bridges between porphyrin units as well as different meso substituents. For quantitative evaluation of the 2PA cross section, we use femtosecond two-

---

* Author to whom correspondence should be addressed. Phone: +1 (406)-994-7831. Fax: +1 (406)-994-4452. E-mail: rebane@physics.montana.edu.
　† Montana State University.
　‡ P. N. Lebedev Physics Institute.
　§ Polish Academy of Sciences.
　|| University of Oxford.
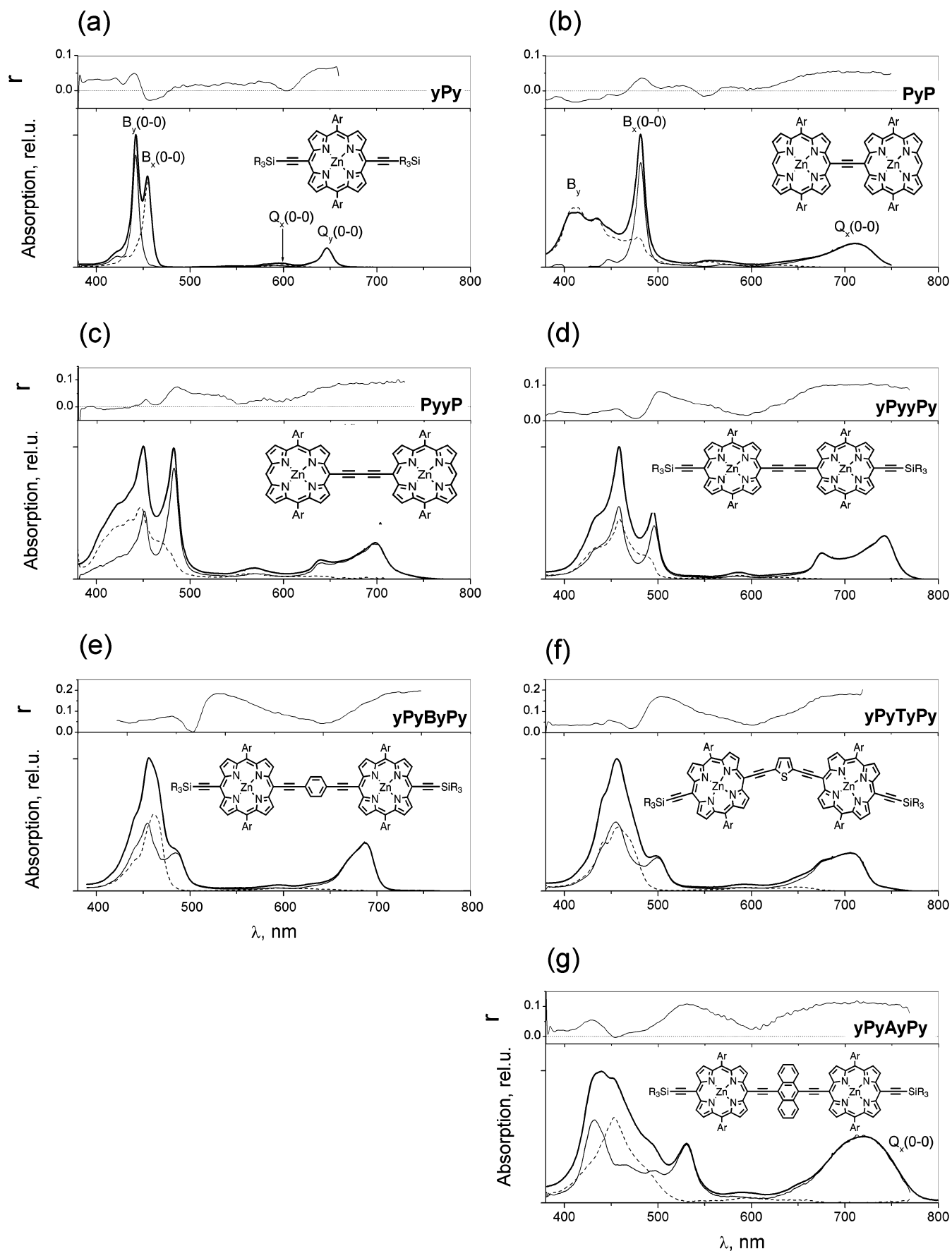
Figure 1. Linear absorption spectra (bold lines) and fluorescence anisotropy as a function of excitation wavelength (top insets) of the studied molecules in 1% pyridine/dichloromethane. The thin continuous line in the absorption spectrum corresponds to transitions, polarized parallel to the longest, fluorescent, transition, and the dashed line corresponds to transitions, polarized perpendicular to it. Chemical structures are shown in insets. In the chemical structures, Ar represents a 3,5-diterbutyl-phenyl group while R represents a hexyl group.

Strong NIR 2PA in Conjugated Porphyrin Dimers

J. Phys. Chem. B, Vol. 109, No. 15, 2005 **7225**

photon excited fluorescence measurement. This is one of the most direct and reliable techniques because the signal is sensitive only to the simultaneous 2PA process and not to other nonlinear optical effects, which can concurrently occur in a sample. Quantitative implementation of the three-level model in describing 2PA in these molecules allows us to extract the important spectroscopic parameters that lead to a drastic enhancement of 2PA in dimers as compared to the monomer. By considering the peak 2PA cross sections of a series of dimers, we formulate important structure−property relationships, which are useful for future design of molecules with an even larger σ_2 value. We also show that these new compounds can generate singlet oxygen upon one- and two-photon excitation with a rather high quantum efficiency, which is very promising for 2PA-induced PDT.

2. Experimental Section

Our laser system comprises a Ti:sapphire femtosecond oscillator (Coherent Mira 900) pumped by a 5 W continuous wave frequency-doubled Nd:YAG laser (Coherent Verdi) and 1 kHz repetition rate Ti:sapphire femtosecond regenerative amplifier (CPA-1000, Clark MXR). The pulses from the amplifier were down-converted with an optical parametric amplifier, OPA (TOPAS, Quantronix), whose output can be continuously tuned from 1100 to 2000 nm. The second harmonic of the OPA idler beam was used for two-photon excitation. The OPA output pulse energy was $100-200$ μJ ($5-10$ μJ after frequency doubling), and the pulse duration was 100 fs.

The collimated excitation laser beam was passed through a pinhole and directed to the sample. The fluorescence emission originating from one- and two-photon excitation was collected with a spherical mirror and focused on the entrance slit of an imaging grating spectrometer (Jobin Yvon Triax 550).

Nonlinear 2PA spectra were obtained by tuning the wavelength of the frequency-doubled OPA output and measuring the relative intensity of the resulting two-photon excited fluorescence.

2PA spectra of the samples were measured relative to Lucifer Yellow in water, whose 2PA spectrum in the same spectral region is known.[13] This allowed us to disregard the dependence of pulse duration and intensity on wavelength. The 2PA cross section of the sample at a wavelength ($\lambda_{ex} = 850$ nm) close to the spectral maximum was then measured, and the whole 2PA spectrum was scaled to that value. The 2PA cross section of the sample (superscript s in the following) was measured by using the relative fluorescence method, based on calibration to both the excitation[14] and registration[15] conditions. Rhodamine B in methanol was used as a reference (superscript r in the following) compound.[13] First, we measured the two-photon excited fluorescence signals of the sample $F_2^{(s)}$ and the reference $F_2^{(r)}$ in their corresponding fluorescence maxima, $\lambda^{(s)}$ and $\lambda^{(r)}$, in exactly the same conditions of excitation and collection geometry. The 2PA cross section of the sample is then expressed as

$$\sigma_2^{(s)}(\lambda_2) = \frac{F_2^{(s)}(\lambda^{(s)})}{F_2^{(r)}(\lambda^{(r)})} \frac{\eta^{(r)}(\lambda^{(r)})}{\eta^{(s)}(\lambda^{(s)})} \frac{\Phi(\lambda^{(r)})}{\Phi(\lambda^{(s)})} \frac{C^{(r)}}{C^{(s)}} \sigma_2^{(r)}(\lambda_2) \quad (1)$$

Here λ_2 designates the wavelength of two-photon excitation, $\eta^{(r,s)}(\lambda)$ is the differential quantum efficiency of fluorescence at λ, $\Phi(\lambda)$ is the collection efficiency of registration system at λ, $C^{(r,s)}$ is the concentration of the substance, and $\sigma_2^{(r)}(\lambda_2)$ is the known 2PA cross section of the reference dye at λ_2. As a next step, we measured one-photon excited fluorescence of the

sample and the reference in the same conditions as upon two-photon excitation but at some wavelength, λ_1, where one-photon absorption (1PA) is present. This allowed us to calibrate our 2PA measurement for an unknown combination of parameters, $\eta(\lambda) \times \Phi(\lambda) \times C$. The ratio of one-photon excited fluorescence signals F_1 of the same pair of substances with low optical densities (OD < 0.1) at λ_1 reads

$$\frac{F_1^{(r)}(\lambda^{(r)})}{F_1^{(s)}(\lambda^{(s)})} = \frac{\eta^{(r)}(\lambda^{(r)})}{\eta^{(s)}(\lambda^{(s)})} \frac{\Phi(\lambda^{(r)})}{\Phi(\lambda^{(s)})} \frac{C^{(r)}}{C^{(s)}} \frac{\sigma_1^{(r)}(\lambda_1)}{\sigma_1^{(s)}(\lambda_1)} \quad (2)$$

where $\sigma_1^{(r,s)}(\lambda_1)$ is the 1PA cross section at λ_1. By combining eqs 1 and 2, we finally get

$$\sigma_2^{(s)}(\lambda_2) = \frac{F_2^{(s)}(\lambda^{(s)})}{F_2^{(r)}(\lambda^{(r)})} \frac{F_1^{(r)}(\lambda^{(r)})}{F_1^{(s)}(\lambda^{(s)})} \frac{\sigma_1^{(s)}(\lambda_1)}{\sigma_1^{(r)}(\lambda_1)} \sigma_2^{(r)}(\lambda_2) \quad (3)$$

Since all of the values in the right-hand side of eq 3 are measured or known, the 2PA cross section of the sample is easily evaluated from eq 3. Note that in this method neither the parameters of the excitation light (pulse energy, pulse duration, spatial and temporal intensity distribution), the parameters of the detection setup (wavelength dependence of the quantum efficiency of the detector and refractive indexes of solvents), nor quantum yield of fluorescence and concentration of the samples need to be known.

Linear absorption spectra were measured using a standard UV−vis spectrophotometer (Perkin-Elmer Lambda 900). Fluorescence excitation spectra and excitation polarization spectra were measured with a luminescence spectrometer (Perkin-Elmer LS 50B). All 2PA as well as 1PA, fluorescence excitation, and polarization spectra were measured in 1% pyridine/dichloromethane solutions at room temperature.

By measuring the dependence of fluorescence anisotropy on the excitation wavelength, we resolved 1PA transitions into components that are either parallel or perpendicular to the lowest fluorescent transition as described in ref 16.

Singlet oxygen photosensitization experiments were performed in 1% pyridine/toluene solution. Singlet oxygen luminescence near 1.27 μm was measured with a nitrogen-cooled Ge detector, coupled to the same grating spectrometer as above (Jobin Yvon Triax 550), upon either one-photon (second harmonic of continuous wave Nd:YAG laser at 532 nm) or two-photon (Ti:sapphire amplifier at 806 nm) excitation of molecules. Quantum efficiency of singlet oxygen photosensitization Φ_Δ was measured upon one-photon excitation relative to tetraphenylporphyrin in toluene at ambient conditions, for which $\Phi_\Delta = 0.68$.[17]

Chemical synthesis of the molecules studied here was described previously.[18,19]

The Hyperchem 7 package was used for the quantum chemical calculations.

3. Results and Discussion

3.1. One-Photon Absorption Spectra and Polarization of Transitions. Since the 2PA properties of tetrapyrroles are intimately connected to their 1PA through the resonance enhancement effect,[8c,d] we first consider one-photon spectroscopy of the series of molecules under investigation.

3.1.1. yPy Monomer. It is known from the previous literature[20−23] that symmetrically bis-*meso*-ethynyl-substituted metalloporphyrin monomers exhibit a substantial red shift and some intensification of the low-energy Q-transition as well as

TABLE 1: Assignment of the Linear Absorption Transitions, According to Their Polarization, for the yPy Monomer

	$S_0 \rightarrow S_1$ $(1^1A_g \rightarrow 1^1B_{2u})$			$S_0 \rightarrow S_2$ $(1^1A_g \rightarrow 1^1B_{3u})$	$S_0 \rightarrow S_3$ $(1^1A_g \rightarrow 2^1B_{3u})$		$S_0 \rightarrow S_4$ $(1^1A_g \rightarrow 2^1B_{2u})$	
polarization (exptl)	0°	0°	0°	90°	90°	90°	0°	0°
transition assignment	$Q_y(0-0)$	$Q_y(0-1)$	$Q_y(0-1')$	$Q_x(0-0)$	$B_x(0-0)$	$B_x(0-1)$	$B_y(0-0)$	$B_y(0-1)$
yPy transition frequency (cm^{-1})	15 460	15 840	16 990	16 670	21 980	23 090	22 620	23 700
yyPyy calculation[21] (cm^{-1})	14 840			15 000	26 780		27 180	

a red shift and splitting (in the case of bis(trialkylsilylethynyl)-substituted molecules[18,23]) of the Soret band. Such behavior has been explained theoretically[21] by a perturbation of the four frontier molecular orbitals due to π-conjugation of the porphyrin electronic system with two ethynylenic groups. As a result, molecular symmetry lowers from D_{4h} to D_{2h}, which results in the splitting of Q- and, in some cases, B-bands. It is important that the classic four-orbital Gouterman model[24] still works for these kinds of monomers and predicts relatively weak (quasi-forbidden) Q-transitions and strongly allowed B-transitions.[21] In some respect, this resembles the type of transformation of the absorption spectrum when passing from unsubstituted metalloporphyrin to its free-base analogue, but in contrast to this latter case, two nonequivalent symmetry axes are directed in the yPy monomer along the axis connecting the two ethynyl substituents (x-axis, by convention) and perpendicular to it (y-axis).

Figure 1a presents the absorption spectrum of the yPy monomer (bottom, bold line). It consists of a group of relatively weak Q-bands in the red region (570−650 nm) and two strong, overlapping B-bands near 450 nm. By measuring the dependence of anisotropy of fluorescence (r) as a function of excitation wavelength (Figure 1a, top), we were able to resolve all of the absorption peaks according to their polarizations with respect to polarization of the lowest, fluorescence transition. The spectrum shown by thin line in Figure 1a, bottom, represents all of the absorption peaks, polarized parallel to the lowest $S_0 \rightarrow S_1$ transition. Absorption, polarized perpendicular to this transition, is shown by dashed line. It is interesting to note that the lowest strong B-band at 21 980 cm^{-1} (455 nm) is polarized perpendicular to the lowest, $S_0 \rightarrow S_1$, transition. The second strong B-band at 22 620 cm^{-1} (442 nm) is polarized parallel to the $S_0 \rightarrow S_1$ transition. Both Q- and B-transitions show several vibronic satellites.

Since the fluorescence polarization spectroscopy provides only information on the relative polarizations of transitions, additional data are needed to fix these directions within the molecular frame. Polarized absorption experiments in stretched polymer film[25] and quantum-mechanical INDO/SCI calculations[21] of similar molecules demonstrate that the lowest-energy $S_0 \rightarrow S_1$ Q-transition is polarized perpendicular to the molecular axis connecting the triple bonds, and therefore, this transition was identified as Q_y. Taking into account our polarization data, we can assign all main absorption peaks in the yPy monomer to $1^1A_g \rightarrow 1^1B_{2u}$ (Q_y at 646 nm), $1^1A_g \rightarrow 1^1B_{3u}$ (Q_x at 595 nm), $1^1A_g \rightarrow 2^1B_{3u}$ (B_x at 455 nm), and $1^1A_g \rightarrow 2^1B_{2u}$ (B_y at 442 nm) transitions, respectively. Note that the experimentally determined energetic sequence of these transitions is correctly reproduced by the INDO/SCI calculation;[21] see Table 1.

3.1.2. Conjugated Dimer Series. Linear absorption spectra of the series of dimers are presented in Figure 1, parts b−g, bold lines. All dimers show some common spectroscopic trends, when compared with the monomer. First, the lowest-energy Q-band is drastically intensified and red-shifted, and second, the Soret (B) band splits over several subbands, whose center also shifts to the red. Similar spectral properties of meso-to-

meso-connected bisporphyrin systems were observed earlier in refs 18−23, 25, and 26. It is noteworthy that the considerable amplification of the Q-band in dimers is one of the key factors governing the enhancement of 2PA response in the near-IR.

In refs 21 and 27−29, it was shown that due to a strong electronic interaction (molecular orbital overlapping) between the two porphyrin macrocycles in dimers the four Gouterman frontier orbitals of the monomer split into at least eight frontier orbitals. This "eight-orbital" model[28] qualitatively describes the complexity of the spectrum and explains the significant intensification of the lowest $S_0 \rightarrow S_1$ (Q) transition. In fact, due to the different, as compared to the monomer, energy positions and symmetries of the frontier orbitals, the lowest Q-transition ceases to be quasi-forbidden by configurational interaction (CI).[28] Another possible reason for the intensification of the Q-transition is an extension of conjugation length simply because of dimerization. However, this latter effect would lead to only a 2-fold increase in oscillator strength,[30] whereas we observe a 4-fold intensification of this transition on going from yPy monomer to yPyyPy dimer (Table 3), which attests the importance of both mechanisms.

To get better insight into the nature of one-photon transitions in this series of porphyrin dimers, we performed polarization analysis, similar to that done for the monomer. The corresponding excitation anisotropy profiles are shown in the top insets to Figure 1, parts b−g. The bands, polarized parallel to the lowest $S_0 \rightarrow S_1$ transition, are shown by the thin solid line and those perpendicular to it by the dashed line. All of the dimers show a qualitatively similar sequence of transitions. Independent polarized absorption experiments in stretched polymer films with a related yyPyyPyy butadiyne-linked dimer[25] have shown that the lowest allowed singlet transition is polarized along the long dimer axis (x) and can therefore be called $Q_x(0-0)$. The same polarization of the lowest singlet transition was obtained with INDO/SCI calculations[21] and with approximate DFT calculations[28] for similar model dimers. Taking into account a topological similarity of molecular wave functions, we thus assume that in all dimers under study the lowest $S_0 \rightarrow S_1$ transition is of the $1^1A_g \rightarrow 1^1B_{3u}$ ($Q_x(0-0)$) type.

Our experiment demonstrates that the lowest, rather strong, $Q_x(0-0)$-transition is followed by its two vibronic satellites, $Q_x(0-1)$ and $Q_x(0-1')$, shifted, depending on particular dimer structure, by 300−600 and 1100−1500 cm^{-1}, respectively, and by a weak, y-polarized, $Q_y(0-0)$ band near 16 000 cm^{-1}. In the Soret region (18 500−24 500 cm^{-1}), there is a group of strong transitions with x- and y-polarizations. Among them, the lowest-energy and relatively narrow peak is always polarized parallel to the $S_0 \rightarrow S_1$ transition, such that we assign it to the $B_x(0-0)$-transition. The second, also relatively narrow, peak with the same polarization is blue-shifted by 1300−2000 cm^{-1} with respect to $B_x(0-0)$ and can be assigned to another B'_x-(0−0) pure electronic transition. For most of the dimers, except PyP and yPyTyPy, there is also a third, broad and relatively weak x-polarized band, which is usually the highest-frequency transition of the Soret group. We tentatively assign this band

TABLE 2: Assignment of Linear Absorption Transitions Frequencies (cm^{-1}), According to Their Polarization, for a Series of Porphyrin Dimers

transition assignment	$S_0 \rightarrow S_1$ $^1A_g \rightarrow {}^1B_{3u}$			$S_0 \rightarrow S_2$ $^1A_g \rightarrow {}^1B_{2u}$	$S_0 \rightarrow S_3$ $^1A \rightarrow {}^1B_{3u}$	$S_0 \rightarrow S_4$ $^1A_g \rightarrow {}^1B_{2u}$	$S_0 \rightarrow S_5$ $^1A \rightarrow {}^1B_{3u}$	$S_0 \rightarrow S_6$ $^1A \rightarrow {}^1B_{2u}$	$S_0 \rightarrow S_7$ $^1A_g \rightarrow {}^1B_{3u}$	$S_0 \rightarrow S_8$ $^1A \rightarrow {}^1B_{2u}$	$S_0 \rightarrow S_9$ $^1A_g \rightarrow {}^1B_{3u}$	$S_0 \rightarrow S_{10}$ $^1A \rightarrow {}^1B_{2u}$
polarization (exptl)	0°	0°	0°	90°	0°	90°	0°	90°	0°	90°	0°	90°
designation	$Q_x(0-0)$	$Q_x(0-1)$	$Q_x(0-1')$	$Q_y(0-0)$	$Q'_x(0-0)$	$Q'_y(0-0)$	$B_x(0-0)$	$B_y(0-0)$	$B'_x(0-0)$	$B'_y(0-0)$	$B_x'(0-1)?$	$B''_y(0-0)$
PyP dimer	14 030	14 730		16 180	17 420	18 050	20 760	21 300	22 420 (0-1)?	22 810		24 300
PyyP	14 310	14 700	15 600	15 890	17 500	17 680	20 730	21 120	22 190	22 320	23 170	23 840
PyyP calculation[28a]	12 500			16 300	19 700		20 900	20 200	19 700			20 600
yPyyPy	13 480	13 990	14 810	15 820	17 090	17 010	20 170	20 530	21 840	21 700	22 810	22 350
yyPyyPy calculation[21]	13 710			14 440			19 360	25 240				
yPyByPy	14 470	14 770	15 150	15 850	16 930	16 490	20 560		22 010	21 630		22 480
yPyTyPy	14 040	14 590	15 560	15 380	16 970	16 800	20 040	21 610	22 040	22 550		
yPyAyPy	13 770	14 540		16 720		17 090	18 870	20 690	20 130	22 080	21 440	22 410

TABLE 3: Summary of Linear Ground-State Absorption, Excess Polarizability for the Lowest S_1 State, Singlet−Singlet Excited-State Absorption, and Two-Photon Absorption Properties of the yPy Monomer and a Series of Dimers

	ground-state absorption						excess polarizability	excited-state absorption		two-photon absorption			
	Q_x $S_0 \rightarrow S_1$			$\sum_i (B_x^{(i)} + B_y^{(i)})$ $S_0 \rightarrow S_n$			$\alpha(S_1) - \alpha(S_0)$	blue transition $S_1 \rightarrow S_m$		blue transition $S_0 \rightarrow S_m$			
molecule	ν_{i0} [a] THz	f_{i0} [b]	$\|\mu_{i0}\|^2$ [c] D^2	ν_{k0} [d] THz	f_{k0} [e]	$\|\mu_{k0}\|^{2}$ [f] D^2	$\Delta\alpha$ Å^3	ν_{fi} [h] THz	$\|\mu_{fi}\|^{2}$ [i] D^2	ν_{f0} [g] THz	Γ [j] (fwhm) THz	ν_{i0}/ν_{f0}	σ_2^{max} [l] GM
yPy	464.4	0.15	20.6	679.8	1.60	150	30 ± 20[23]	242.1	150	706.5	87.6	0.657	20
PyP	421.3	0.35	52.2	689.3	2.91	269	460[22]	306.2	1600	727.5[k]	56.5	0.579	8600[k]
PyyP	429.9	0.38	56.4	675.4	3.33	315		288.6		718.5	42.4	0.598	5500
yPyyPy	404.4	0.58	91.5	663.4	3.03	291	400 ± 40[23]	274.9	1350	679.3	47.3	0.595	9100
yPyByPy	436.8	0.52	76.0	662.6	3.03	292	270 ± 30[23]	247.6	860	684.4	83.0	0.638	3800
yPyTyPy	424.2	0.58	87.2	660.8	3.15	304	390 ± 40[23]	253.7	1200	674.2	67.4	0.629	3100
yPyAyPy	417.9	0.64	97.7	660.3	2.36	228	590 ± 60[23]	295.8	900	713.7[k]	44.8	0.586	10 100[k]

[a] Central frequency. [b] Oscillator strength. [c] Transition dipole moment squared of the lowest Q-transition (all obtained by integration over corresponding 0−0 and vibronic bands). [d] Central frequency. [e] Oscillator strength. [f] Transition dipole moment squared of the Soret multiplet (all obtained by integration over the entire Soret region). [g] Frequency of the blue 2PA peak; see text for definition. [h] Frequency and [i] transition dipole moment squared of the excited-state transition, corresponding to the blue 2PA peak (see eq 12 and below for definition of these quantities). [j] Spectral width of the 2PA transition, found by using Gaussian (or two Gaussian) fits to experimental data presented in Figure 3. [k] Found by extrapolation of the Gaussian fit to 2PA spectrum in Figure 3. [l] Maximum 2PA cross section, observed experimentally (from Figure 2).
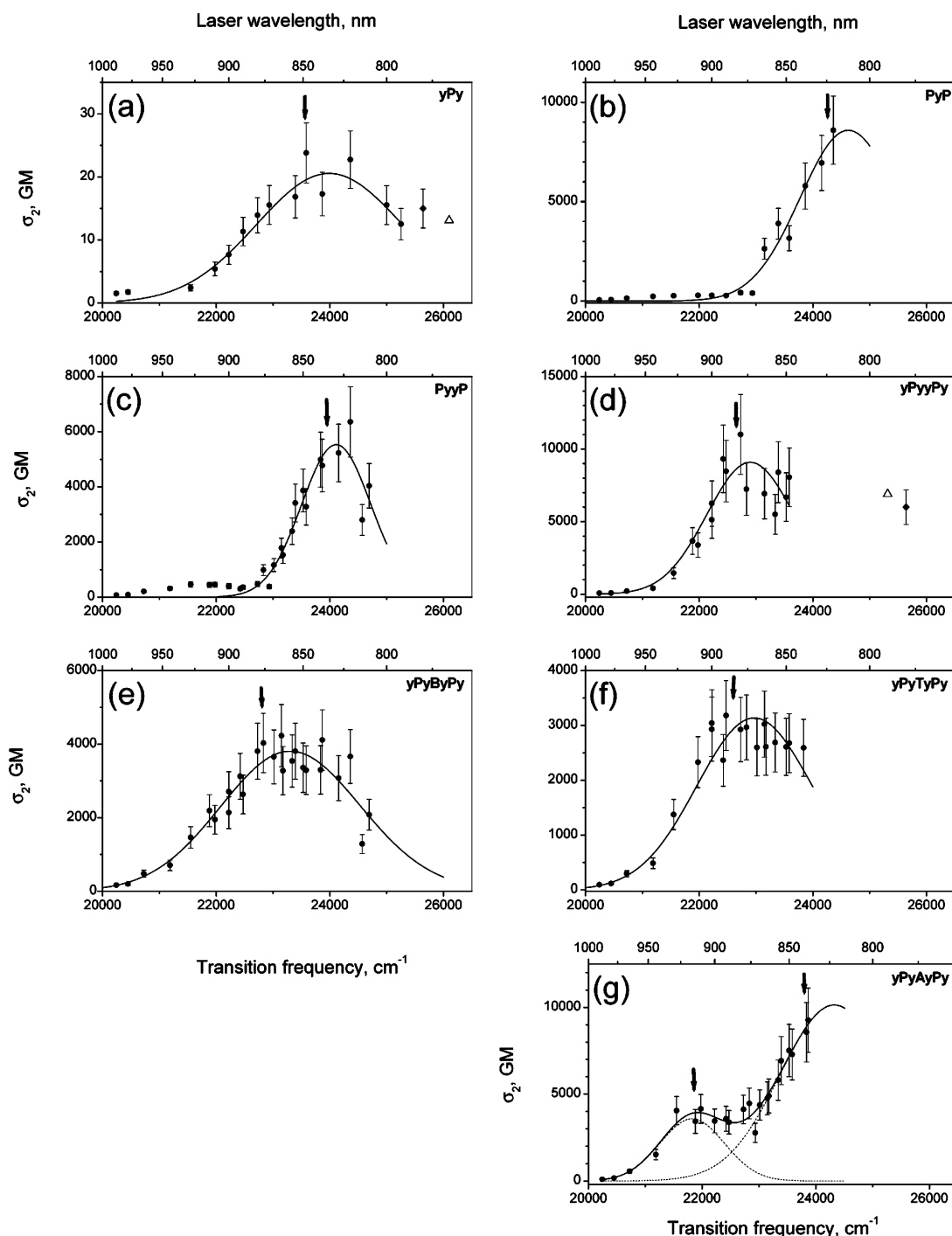
Figure 2. Absolute two-photon absorption spectra (filled circles) of the studied molecules. A short arrow indicates the frequency of molecular 2PA transition, ν_{f0}, which is obtained from Figure 3. The shift of this frequency from the real peak position is due to the resonance enhancement effect. The solid line corresponds to the best Gaussian(s) fit to the data, presented in Figure 3, divided over the detuning factor $(\nu - \nu_{i0})^2$; see text. Other symbols shown in Figure 2 are explained in the text.

to a vibronic satellite of the B'_x transition, since it is relatively weak and shifted by ~ 1000 cm^{-1} to higher energies with respect to $B'_x(0-0)$.

Several broad and relatively strong, y-polarized B_y-bands span a wide region to the blue from the $B_x(0-0)$-transition.

An assignment of all of the observed bands to particular transitions occurring between eight frontier orbitals, mixed via configuration interaction, can be done only with a very limited confidence because of the complexity of the system. We, however, present here a tentative assignment of some transitions in the PyyP dimer, by comparing our results in Table 2 with the simplified DFT calculation performed in ref 28a. Semiem-

pirical calculation that takes into account CI[21] gives a generally similar and complex structure in the Soret region of the yyPyyPyy dimer. Even though we cannot confidently assign all of the transitions in the Soret multiplet at this moment, it turns out that our analysis of frequencies and polarizations of one-photon transitions will suffice for the purposes of quantitative analysis of 2PA, as presented in the next section.

Several integral 1PA parameters, relevant for the following consideration of 2PA, are summarized in Table 3.

3.2. Two-Photon Absorption Spectra. 2PA spectra of all of the molecules under investigation are presented in Figure 2, parts a−g. For all of the 2PA experimental data points, we

Strong NIR 2PA in Conjugated Porphyrin Dimers

J. Phys. Chem. B, Vol. 109, No. 15, 2005 **7229**

confirmed that fluorescence intensity had a quadratic dependence on the laser power. At excitation frequencies higher than those presented in Figure 2, this dependence gradually declined from quadratic and became linear because hot-band absorption started to compete with 2PA.[8f,g]

In the following discussion, we will be interested in the position of real 2PA energy levels (corresponding to molecular eigenstates) and cross sections at these energies. Figure 2 presents, however, raw data where the peak position can be blue-shifted with respect to the real 2PA level because of the resonance enhancement, occurring when the excitation laser frequency, ν, approaches from below the frequency ν_{i0} of the first Q(0−0)-transition. The applicability of this single intermediate state approximation has been shown by us before for several tetrapyrrolic molecules[8c−e] and is validated further in the text for the molecules under study (section 3.3). Thus, to separate the real spectral shape of the 2PA transition from the resonance enhancement effect, we present, similar to what was done in ref 8d, the 2PA spectrum in $\sigma_2(2\nu)$ $(\nu_{i0} - \nu)^2$ versus 2ν coordinates in Figure 3. Then, we fit the experimental data in Figure 3 to one or two Gaussians and use the thus obtained maximum frequency, cross section at this frequency, and width for comparison with theory. The smooth curves in Figure 2 represent the ratio of the Gaussian fit, obtained from Figure 3, divided by the detuning factor $(\nu_{i0} - \nu)^2$.

3.2.1. yPy Monomer. We start our consideration with the 2PA spectrum of a model monomer compound, yPy monomer in dichloromethane solution, Figures 2a and 3a, filled circles. A filled diamond in Figure 2a presents our previous datum obtained for the same molecule in a polymer film at 780 nm excitation.[8g]

Considering the 2PA spectrum of yPy, several important features have to be noted:

(1) A discernible 2PA peak is observed at 23 550 cm^{-1} (Figure 3a).

(2) This peak, blue-shifted with respect to the one-photon Soret band, does not reproduce any other 1PA feature.

(3) Its full width at half-maximum (fwhm) is rather large (2900 cm^{-1}), as compared to similar peaks in ethyne- and butadiyne-bridged dimers (see below).

A maximum cross section value, $\sigma_2 = 20 \pm 5$ GM (Figure 2a), is moderate and of the same order of magnitude as that was found in this spectral region for other porphyrin monomers not bearing strong electron donor or acceptor substituents.[8e,f]

Since the yPy monomer possesses a center of inversion (D_{2h} group of symmetry), selection rules for one- and two-photon transitions should be alternative, such that the one-photon-allowed electronic transitions are forbidden for 2PA and vice versa. This is confirmed by our experiment (observation 2), suggesting that we deal with gerade−gerade type transition(s) in this monomer. It is worth noting that quantum-mechanical INDO/MRD-CI calculation of an yyPyy porphyrin[21] predicts several weak singlet−singlet excited-state transitions, originating from the 1^1B_{2u} state (which is the dominant intermediate state in 2PA), in the spectral region studied here. By adding the calculated[21] $S_1 \rightarrow S_n$ transition energy to experimental Q$_y$ (0−0) energy, we obtain the corresponding 2PA spectrum and present it as a bar graph in Figure 3a in relative values. Two close-lying $S_1 \rightarrow S_n$ transitions, which are relatively well-separated from the other higher-frequency transitions, can be associated with an experimentally observed 2PA band, although the calculated energies are slightly overestimated. Given that the 1PA Soret transition energies are also overestimated in this calculation, the theoretical results seem reasonable and quali-

tatively explain the observed position and width of the 2PA band. More important is that the excited-state absorption, responsible for the 2PA peak at 23 550 cm^{-1}, is predicted to be rather weak, with an oscillator strength of ∼0.1, which accounts for the relatively weak 2PA cross section of the monomer (see below).

We also present in Figure 2a an absolute σ_2 value (13 GM) obtained by ZINDO−CI/SOS quantum-mechanical calculations for a yPy-type monomer at excitation wavelength 770 nm (open triangle).[32] The authors of that article do not present the frequencies of the individual 2PA transitions but rather an averaged envelope spectrum, which peaks at a $2\nu = 31\,830$ cm^{-1} transition frequency. However, their data point at 770 nm quantitatively correlates with our experiment.

3.2.2. Conjugated Dimer Series. Figure 2, parts b−g, and Figure 3, parts b−g, show the 2PA spectra of the dimers. All of the spectra comprise a very strong 2PA peak with a transition maximum lying, depending on the particular compound, in the region 22 500−24 500 cm^{-1}. We call this high-frequency transition the "blue" peak. We should emphasize that the cross section values observed here for porphyrin dimers amount to several thousand Göppert−Mayer units, which are extremely high for molecules of this size. In the PyP and yPyAyPy dimers, we could not actually reach a real spectral maximum, because strong 1PA starts to compete with 2PA upon shifting excitation to a higher frequency. Nevertheless, we were able to estimate the blue peak maximum frequency and σ_2 value from the best Gaussian fits to these spectra. It is interesting to note that the blue peak frequency thus obtained for the PyP dimer (24 250 cm^{-1}) is very close to the sum of the 1PA (Q$_x$(0−0)) transition frequency (14 030 cm^{-1}) and the frequency of the strong transient singlet−singlet absorption peak (10 150 cm^{-1}), published in ref 33 for the same molecule. This suggests that the simultaneous 2PA, measured here, and femtosecond stepwise singlet−singlet absorption, reported in ref 33, most probably populate the same final state of the PyP dimer.

In addition to the blue peak, PyP, PyyP, and yPyAyPy dimers also show a weaker transition at lower frequencies, near 21 000−22 000 cm^{-1}, which we call a "red" peak. For the PyP, PyyP, and yPyAyPy spectra, we applied a two-Gaussian fit, shown by full line in Figure 3, parts b, c, and g. For the rest of the dimers, a single-Gaussian fit works well and is shown in Figure 3, parts a and d−f, by a full line. The values of the transition maximum, spectral width (fwhm), and peak cross section obtained from the best Gaussian fits to the 2PA transitions of all molecules are collected in the right-hand side of Table 3.

Concerning the 2PA spectra of the dimers, it is obvious from Figure 3, parts b−g, that the lowest one-photon Soret B$_x$(0−0)-transition is never reproduced in 2PA. This suggests that the selection rules for one- and two-photon transitions are alternative in dimers, similar to the case of the monomer. While in the monomer the inversion symmetry of molecule is beyond question, in dimers two porphyrin rings can adopt mutually noncoplanar geometry in solution, which, generally speaking, can break the inversion symmetry of the whole molecule. The question about possible twisting of porphyrin rings in alkynyl-bridged dimers is widely discussed in the literature. For several dimers studied here, X-ray analysis shows almost coplanar conformation in crystals,[26b,34] but in solution it can be different, especially for the PyP dimer, where steric clash between the closely neighboring β-hydrogens of the two porphyrin rings can distort the molecule from perfect planarity.[33,35] Our semiem-
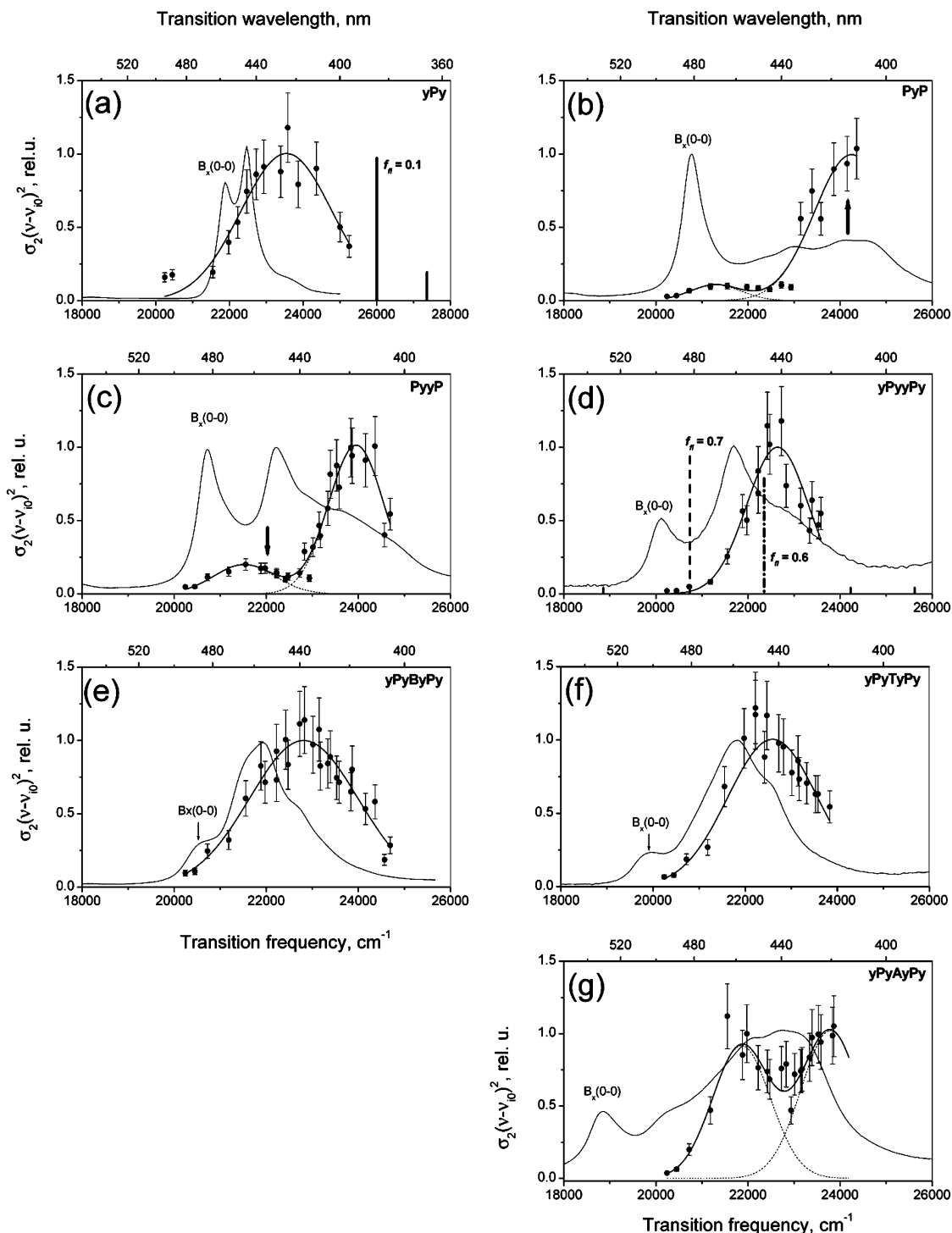
Figure 3. Spectral profiles of the 2PA transitions, corrected for the resonance enhancement effect (solid circles with best Gaussian fits). The thin solid line presents the 1PA spectrum in the same spectral region. The lowest Soret transition is indicated by $B_x(0-0)$. Two bars in Figures 3a correspond to two excited-state singlet−singlet transitions, calculated in ref 21 for yyPyy. The bars in Figure 3d correspond to excited-state singlet− singlet transitions, calculated in ref 21 for yyPyyPyy in the case of cumulenic geometry of the bridge (dashed line) and to strongly alternating geometry (dash−dotted line). An arrow in Figure 3c points to a frequency of a gerade state obtained in this region by the DFT calculation of a PyyP dimer.[31] An arrow in Figure 3b indicates a position of the 2PA transition, calculated from the excited-state transition maximum, experimentally found for this molecule in ref 33.

pirical AM1 geometry optimization calculations have shown that in the ground electronic state the dihedral angle between porphyrin planes is equal or less than 20° in all of the dimers, except the PyP dimer, where it is 36° (cf. ref 33). The noncoincidence of the 1PA $B_x(0-0)$-transition with any 2PA transition and the general similarity of the 2PA spectra of all of the dimers implies that all of these molecules are effectively centrosymmetric (predominantly coplanar) in solution and their

electronic states can be assigned either to gerade or to ungerade types of "D_{2h}-like"[36] groups of symmetry. It is interesting that this seems to apply also to the yPyTyPy dimer, where, independent of torsion angle, the molecule is, strictly speaking, asymmetrical because of the asymmetric bridge structure. However, the global symmetry of the system is, probably, only slightly perturbed, and it can still be described in terms of a D_{2h}-like group.

Strong NIR 2PA in Conjugated Porphyrin Dimers

J. Phys. Chem. B, Vol. 109, No. 15, 2005 **7231**
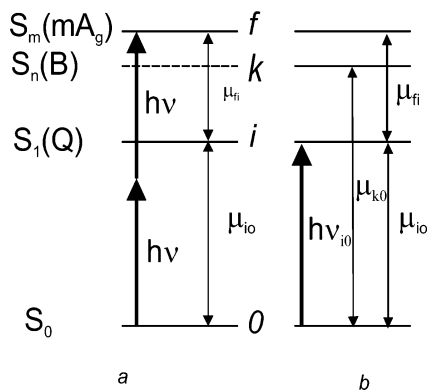
Figure 4. (a) Three-level model system, used for description of the 2PA. 0 designates the ground state, i is the intermediate, one-photon-allowed (Q) state, and f is the 2PA-allowed final state. In some molecules, we observe two final states, corresponding to the blue and red peaks in the 2PA spectrum. (b) Four-level model system, used for description of the ground- and excited-state polarizability. In addition to the three-level system (shown in part a), the one-photon-allowed state k (Soret manifold) is introduced here to describe more accurately the ground-state polarizability.

Therefore, we can state that the first reason for the extremely large 2PA cross section in dimers is that the transition that we are dealing with is of the gerade−gerade type, and therefore, it is 2PA-allowed.

The excited-state absorption spectrum, originating from the lowest excited, $1B_{3u}$ state of a yyPyyPyy dimer was calculated with the INDO/MRD-CI technique in ref 21. In these calculations, the dimer geometry was assumed to be coplanar, but an alternation of single and triple bonds in the bridge was chosen to be either strong or weak. In both cases, gerade states were found in the region of our experimental measurements. We compare in Figure 3d these results with our experimental data for yPyyPy. Dashed lines correspond to weakly alternating (cumulenic) geometry and dash−dotted lines to strongly alternating geometry. A relatively strong, well-isolated transition is found for both geometries very close to the experimental peak. What is most important for our further consideration of 2PA enhancement in porphyrin dimers is that the oscillator strength of this transition is about an order of magnitude larger than that found for the yPy monomer (i.e., 0.7 vs 0.1).

The absolute 2PA cross section of a molecule very similar to yPyyPy was calculated in ref 32. Again, the authors present only an envelope spectrum, which peaks at $\lambda_{exc} = 739$ nm (27 060 cm^{-1} transition frequency). Their datum at 790 nm, represented by an open triangle in Figure 2d, falls close in magnitude to our experiment, especially if we compare it to our previous result[8g] shown by the filled diamond, which was obtained at $\lambda_{exc} = 780$ nm in a polymer film.

3.3. Three-Level Model Description of 2PA. To describe the 2PA process on a quantitative level, we now consider a simple three-level model, schematically presented in Figure 4a, and encompassing the ground (0), intermediate (i), and final (f) states. Following our previous papers,[8c−e] we identify the single intermediate i-state with the lowest Q-state (including pure electronic and vibronic levels). For the yPy monomer, this corresponds to the B_{2u} Q_y-state and for all of the dimers to the B_{3u} Q_x-state. The final state in our model is a gerade state, which for D_{2h} group of symmetry can be either of the A_g or B_{1g} type. For PyP, PyyP, and yPyAyPy dimers, we consider here two different final states, related to the above red and blue 2PA peaks.

All our data, presented above in section 3.2, suggest that the f-state in dimers is rather well-isolated from other gerade states

and possesses a definite line width, which is determined by homogeneous and/or inhomogeneous broadening.

The 2PA spectrum of the yPy monomer (Figure 3a) is also described well by a single peak, with, however, a somewhat larger width. This broadening could be due to two gerade transitions, merging in one band, as discussed above. In this case, we can consider the quasi-degenerate final level also as an isolated state connected to the intermediate i-state by some "effective" (combined) transition dipole moment.

For the centrosymmetric molecule with three essential states, the 2PA cross section can be obtained in second-order perturbation theory[37] as follows

$$\sigma_2 = 2\frac{(2\pi)^4\nu^2L^4}{(hc)^2n^2}\frac{(\mu_{i0}\mathbf{e})^2(\mu_{fi}\mathbf{e})^2}{(\nu_{i0}-\nu)^2+(\Gamma_i/2)^2}g(2\nu) \qquad (4)$$

Here ν is the laser frequency, n is the refractive index of the medium, L is the Lorentz local field factor, calculated as $L = (n^2 + 2)/3$, $\mathbf{e}$ is the unit laser polarization vector, Γ_i is the line width (fwhm) of the ith state, and $g(2\nu)$ is the normalized 2PA line shape function (in Hz^{-1}), such that

$$\int_{-\infty}^{\infty} g(2\nu)\,d(2\nu) = 1$$

The value of σ_2 in eq 4 is twice that originally presented in ref 37 (eq 12.5.40 of ref 37). This is because of different definitions of the 2PA cross section used here and in ref 37. Our definition of σ_2 corresponds to that most commonly used in experimental literature and reflects the fact that two photons are needed to excite one molecule[13]

$$R_{f0}^{(2)} = \frac{1}{2}\sigma_2 I^2 \qquad (5)$$

Here $R_{f0}^{(2)}$ is the molecular transition rate and I is the photon flux (eq 12.5.39 of ref 37). Spatial averaging of eq 4 over all possible molecular orientations[38] results in

$$\sigma_2 = 2\frac{(2\cos^2\theta + 1)}{15}\frac{(2\pi)^4\nu^2L^4}{(hc)^2n^2}\frac{|\mu_{i0}|^2|\mu_{fi}|^2}{(\nu_{i0}-\nu)^2+(\Gamma_i/2)^2}g(2\nu) \qquad (6)$$

where θ is the angle between transition dipole moments μ_{i0} and μ_{fi}. Since the first $(0 \rightarrow i)$ one-photon transition in porphyrin dimers is polarized along the x-axis $(1A_g \rightarrow 1B_{3u})$, $\theta = 0°$ corresponds to the second $(i \rightarrow f)$ transition of the $1B_{3u} \rightarrow A_g$ type polarized along the x-direction, and $\theta = 90°$ corresponds to the second transition of the $1B_{3u} \rightarrow B_{1g}$ type, which is y-polarized. In yPy, the first transition $(1A_g \rightarrow 1B_{2u})$ is polarized perpendicularly to the long molecular axis. Therefore, in this case $\theta = 0°$ corresponds to the second transition of the $1B_{2u} \rightarrow A_g$ type, polarized along y-axis, and $\theta = 90°$ corresponds to the x-polarized $1B_{2u} \rightarrow B_{1g}$ transition.

For the maximum σ_2 value of the Gaussian 2PA peak and specific values of θ (0° or 90°), eq 6 can be further simplified, as follows

$$\sigma_2^m = \frac{(2\pi)^4}{5}\sqrt{\frac{\ln 2}{\pi}}\frac{L^4}{(hc)^2n^2}\frac{|\mu_{i0}|^2|\mu_{fi}|^2}{\left(\frac{\nu_{i0}}{\nu_{f0}}-\frac{1}{2}\right)^2+\left(\frac{\Gamma_i}{2\nu_{f0}}\right)^2}\frac{1}{\Gamma_f}$$

$$\text{for } \theta = 0° \quad (7a)$$

$$\sigma_2^m = \frac{(2\pi)^4}{15}\sqrt{\frac{\ln 2}{\pi}}\frac{L^4}{(hc)^2 n^2}\frac{|\mu_{i0}|^2|\mu_{fi}|^2}{\left(\frac{\nu_{i0}}{\nu_{f0}}-\frac{1}{2}\right)^2+\left(\frac{\Gamma_i}{2\nu_{f0}}\right)^2}\frac{1}{\Gamma_f}$$

$$\text{for } \theta = 90° \quad (7b)$$

From our one- and two-photon absorption measurements, we know all of the molecular parameters in eq 7, except the i → f transition dipole moment squared $|\mu_{fi}|^2$. This latter value is accessible by different techniques, including femtosecond- and picosecond-pump−probe spectroscopy, electroabsorption (Stark effect), and flash photolysis time-resolved microwave conductivity (FP-TRMC). The last two methods give the value of the excess molecular polarizability, $\Delta\alpha$, defined as a polarizability difference between the first excited i-state and the ground state

$$\Delta\alpha = \alpha_i - \alpha_0 \quad (8)$$

Since the excited-state polarizability α_i is intimately connected to the transition dipole moments from the i-state to the closest neighboring states, the $|\mu_{fi}|^2$ value can be deduced from $\Delta\alpha$.

The $\Delta\alpha$ values of all of the molecules studied here (except the PyyP dimer) were measured with either electroabsorption[22] or FP-TRMC techniques[23] and are collected in Table 3. To obtain the $|\mu_{fi}|^2$ values, we consider a four-essential-level model, shown in Figure 4b. In addition to the three levels, used for description of 2PA, it also comprises a one-photon accessible Soret state, depicted as state k. In the case of the PyP and yPyAyPy dimers, we had to consider even a fifth state, which is the red 2PA-allowed state near 22 000 cm^{-1} (Figure 3, parts b and g), contributing significantly to α_i. By using the general relationship[39]

$$\alpha_m = \frac{2}{3}\sum_n \frac{|\mu_{nm}|^2}{h\nu_{nm}} \quad (9)$$

we find within our four-essential-states model

$$\alpha_0 = \frac{2}{3}\left[\frac{|\mu_{i0}|^2}{h\nu_{i0}} + \frac{|\mu_{k0}|^2}{h\nu_{k0}}\right] \quad (10)$$

and

$$\alpha_i = \frac{2}{3}\left[\frac{|\mu_{fi}|^2}{h\nu_{fi}} - \frac{|\mu_{i0}|^2}{h\nu_{i0}}\right] \quad (11)$$

By combining eqs 8, 10, and 11, we obtain

$$|\mu_{fi}|^2 = h\nu_{fi}\left(\frac{3}{2}\Delta\alpha + 2\frac{|\mu_{i0}|^2}{h\nu_{i0}} + \frac{|\mu_{k0}|^2}{h\nu_{k0}}\right) \quad (12)$$

A derivation of the analogous equation for the five-state model, applicable to PyP and yPyAyPy dimers, is straightforward.[40] By using all experimental data, collected in Table 3, and taking $\nu_{fi} = \nu_{f0} - \nu_{i0}$, we calculate $|\mu_{fi}|^2$ according to eq 12 and show the results in Table 3. At this point, we should note that the values of $|\mu_{fi}|$ obtained for the dominating (blue) 2PA transitions are extremely large in these dimers, amounting to 30−40 D. The possible origin of this gigantic transition strength is discussed further in the text.

With this information in hand, we present all of the molecular parameters, entering the right-hand side of eq 7, as well as their combination, $X = |\mu_{i0}|^2|\mu_{fi}|^2\Gamma_f^{-1}(\nu_{i0}/\nu_{f0} - \frac{1}{2})^{-2}$, in Table 4 and plot σ_2^m against X in Figure 5. If the three-level 2PA model

works for the series of molecules under study, this plot should represent a linear function $\sigma_2^m = AX$, where A is a constant factor, defined according to eq 7, which depends only on fundamental constants, solvent properties, and mutual orientation of vectors μ_{i0} and μ_{fi}. For dichloromethane, with $n = 1.424$, we obtain $A = 3.475 \times 10^{32}$ esu for parallel μ_{i0} and μ_{fi} and $A = 1.158 \times 10^{32}$ esu for perpendicular μ_{i0} and μ_{fi}. Both $y = AX$ lines are shown simultaneously in Figure 5. Note that these are theoretical lines without any fitting parameters. If one assumes that μ_{i0} and μ_{fi} are parallel, then there is a very good quantitative agreement between experiment and theory for all dimer data, including both red and blue 2PA transitions. This suggests that the final 2PA states of the dimers possess A_g-like symmetry. For the yPy monomer, the absolute σ_2 value corresponds better to the perpendicular alignment of μ_{i0} and μ_{fi}. However, a rather large experimental error does not exclude the parallel arrangement of transition dipoles as well.

Another important conclusion stemming from Figure 5 is that the three-level model is quite sufficient to describe the 2PA process, and the four-level model (five-level for PyP and yPyAyPy dimers) is sufficient for quantitative description of the excess polarizability for all of the molecules studied here.

Now we turn our attention to different factors, which make the 2PA cross section in the dominant peak of the dimers so large. Table 4 summarizes several spectroscopic molecular parameters, which contribute to the value of X. First of all, we see that the intermediate Q-transition intensity, $|\mu_{i0}|^2$, increases in dimers by 2.5−5 times compared to the monomer. The nature of this enhancement has been discussed in section 3.1 and is due to both perturbation of the four-orbital model and elongation of π-conjugation. As for the role of variations in chemical structure of the dimers, it is evident that $|\mu_{i0}|^2$ roughly follows the conjugation length of the molecule. In particular, it increases in the series PyP < PyyP < yPyyPy. For dimers having the same side substituents but different bridges, it increases in the series yPyByPy < yPyTyPy < yPyyPy < yPyAyPy. It is interesting that the same tendency is also observed for the second transition dipole moment squared, $|\mu_{fi}|^2$, and the excess polarizability, $\Delta\alpha$.[23] The preference of diethynylanthracene over the diethynylbenzene bridge, observed here, can be explained in terms of better charge-passing ability of the former, found in recent theoretical work.[41] A connection of the (symmetrical) charge-transfer effect to the strength of excited-state transition is discussed below. The fifth column in Table 4 shows a frequency detuning factor, which depends on the ratio of one- and two-photon transition frequencies in the three-level system. By its definition, this factor increases drastically when the ratio ν_{i0}/ν_{f0} tends to 0.5. However, in this limiting case, 1PA will dominate the optical response at reasonable laser intensities, thus making 2PA immaterial for practical applications. The detuning factor is 1.4−5 times larger in dimers than that in the monomer. It is interesting to note that the smallest, PyP dimer, shows the optimum detuning factor with $\nu_{i0}/\nu_{f0} = 0.579$.

The fourth column of Table 4 represents an inverse line width of the 2PA transition. This value changes only slightly and not systematically in dimers, becoming 1.5−2 times that of monomer. The narrowing of the 2PA bands in the dimers, compared to those of the monomer, can be due to a spectral focusing of several 2PA states into a single dominant one upon linear elongation of the system.

At the same time, the dipole moment squared of the i → f transition is also dramatically enhanced (6−11 times) in dimers, as presented in the third column of Table 4. It is interesting to note that the corresponding oscillator strengths reach gigantic

Strong NIR 2PA in Conjugated Porphyrin Dimers

J. Phys. Chem. B, Vol. 109, No. 15, 2005 **7233**

TABLE 4: Summary of the Factors Entering the Right-Hand Side of Equation 7 and the 2PA Cross Section Measured at the Frequency of the Two-Photon Transition,$\nu_{f0}{}^a$

molecule	$|\mu_{i0}|^2$ (D^2)	$|\mu_{fi}|^2$ (D^2)	Γ_f^{-1} (THz^{-1})	$(\nu_{i0}/\nu_{f0} - {}^1\!/_2)^{-2}$	$|\mu_{i0}|^2|\mu_{fi}|^2\Gamma_f^{-1}(\nu_{i0}/\nu_{f0} - {}^1\!/_2)^{-2}$ ($\times 10^{-79}$ esu)	$\sigma_2(\nu_{f0})$ ($\pm25\%$) (GM)
yPy	20.6	147	0.011	40	0.13	19
PyP(b)	51.7	1460	0.018	160	22	7800
PyP(r)	51.7	140	0.026	39	0.73	255
PyyP(b)	56.4		0.024	102		5400
PyyP(r)	56.4					480
yPyyPy	91.5	1350	0.021	110	29	8700
yPyByPy	76.0	860	0.012	53	4.2	3500
yPyTyPy	87.2	1200	0.015	64	10.0	2900
yPyAyPy(b)	97.7	900	0.022	137	27	8700
yPyAyPy(r)	97.7	900	0.023	53	10.7	3900

^{a} See text for definition of ν_{f0}.
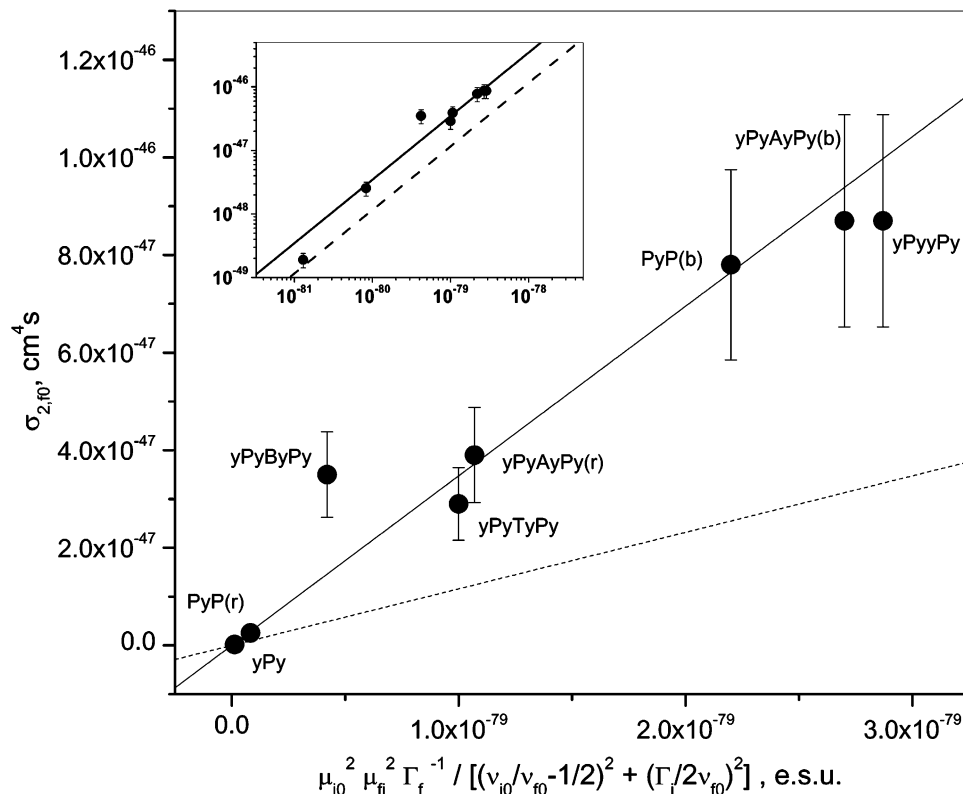
Figure 5. Dependence of the maximum 2PA cross section on a combination of other molecular parameters, measured independently. The straight lines present a theoretical relation between σ_2 and this combination of parameters, obtained in the three-level approximation without any fitting parameters. The solid line corresponds to a parallel arrangement of dipoles of two real consecutive transitions and the dashed line to a perpendicular arrangement. Indexes b and r correspond to the blue and red 2PA peaks, respectively; see text. The inset shows the same plot on a double logarithmic scale.

values. For example, for PyP dimer, $f_{fi} \approx 8$. In many cases, a reasonable estimation of the maximum oscillator strength in a system of fully conjugated N_π π-electrons results from a simple, "particle-in-a-box" model.[30] This model gives for an excited-state, HOMO + 1 → HOMO + 2, $\pi \to \pi^*$, transition

$$f_{fi} = \frac{8}{3\pi^2}\cos^2\!\left(\frac{\beta}{2}\right)N_\pi \qquad (13)$$

where $180° - \beta$ is the valency angle between successive chain links and N_π is considered to be much larger than 1. Taking $\beta = 60°$ for a C−C=C− conjugated system, we get $f_{fi} \approx 0.2N_\pi$. Experimental oscillator strength values obtained here for conjugated porphyrin dimers vary from 3 to 8, which constitute a considerable part of the above theoretical limit, which is $f_{fi} \approx 10$ (for $N_\pi \approx 50$), thus showing that the i → f transition is strongly allowed.

We believe that the nature of this gigantic oscillator strength in our porphyrin dimers is similar to that previously found in a wide range of one-dimensional π-conjugated oligomer and polymer systems. In particular, it was shown[42] that, starting from some critical chain length, the $1B_u \to mA_g$ transition (m designates an unknown chain length and Coulomb correlation dependent quantum number) can concentrate the overwhelming majority of absorption originating from $1B_u$. For example, for *trans*- and *cis*-polyenes, oligofurans, and oligothiophenes, this critical length was found to be ~12 Å.[42k,l] As a result of such unusual properties (gigantic oscillator strength concentrated in one transition), the mA_g state appears to be one of the essential states in the third-order nonlinear response of such molecules.[42a,b,d,f,g,m] The energy of the mA_g state varies in linear oligomers between 1.4 and 1.8 times the energy of the $1B_u$ state.[42f,h,k,l] In our designations, this means that $\nu_{i0}/\nu_{f0} = 0.56-0.71$.

An alternative (with respect to the particle-in-a-box model) explanation of the gigantic oscillator strength of the $1B_u \rightarrow mA_g$ transition can be presented by describing a linear π-conjugated system with an one-dimensional semiconductor model. In this case, the $1B_u \rightarrow mA_g$ transition is associated with a long-distance charge transfer from the one end of the molecular chain to the other.[42b] Of course, because of molecular centrosymmetry, the actual charge density in both the $1B_u$ and the mA_g states is symmetric with vanishing dipole moments. In terms of semiconductor physics, the mA_g states correspond to impurity levels lying slightly below the conduction band and therefore concentrating a huge oscillator strength (for transition from low-lying odd states) because of their large delocalization radius (large electron–hole separation).[43]

The dominant 2PA state in the porphyrin dimers demonstrates a set of special features of the mA_g state, inherent in one-dimensional molecular systems. Namely, it is of the A_g symmetry and extremely strong (fully allowed) for transition from the $1B_{3u}$ and seems to be well-isolated from the other 2PA states, and its energy is 1.6–1.8 times that of the lowest one-photon transition. The linear extension of the π-conjugated system along the x-axis is large, being 18–25 Å for the most separated meso carbons (our AM1 calculation) resulting in a quasi-one-dimensionality of the molecule. Furthermore, mA_g states in the same spectral region were assumed earlier[44] to explain the enhancement of the real part of the third-order susceptibility in similar butadiyne-linked conjugated porphyrin oligomers. All of these data strongly suggest that we are dealing with a 2PA transition, terminating at an mA_g-type state in this series of dimers.

Concluding this section, we can list the main factors, which give rise to a dramatic enhancement of 2PA in porphyrin dimers, as compared to the corresponding monomer:

(1) The first one-photon-allowed Q-transition in dimers ceases to be quasi-forbidden by configurational interaction (CI) and further intensifies due to a larger π-conjugation pool.

(2) The relative energies of one-photon $1B_{3u}$ and two-photon mA_g states are very favorable, such that their ratio is $\nu_{i0}/\nu_{f0} = 0.58$–0.64 in dimers. This drives the three-level system close to strong resonance enhancement, while still keeping 1PA from becoming detrimentally strong (at $\nu_{i0}/\nu_{f0} = 0.5$).

(3) The excited-state transition $1B_{3u} \rightarrow mA_g$ in dimers becomes extremely strong and spectrally concentrated due to the quasi-one-dimensional elongation of the system.

(4) An additional factor of 3 in enhancement comes from the fact that the two consecutive transitions, $S_0 \rightarrow S_1$ and $S_0 \rightarrow S_m$ are polarized parallel to each other in dimers (ref 33 for yPy), while they are most probably perpendicular in the monomer.

3.4. Singlet Oxygen Generation upon One- and Two-Photon Excitation of Conjugated Porphyrin Dimers. One of the most promising applications of the gigantic 2PA efficiency found here in the near-IR could be two-photon-induced photodynamic therapy. The key photophysical process of PDT is generation of singlet molecular oxygen, following two-photon excitation of a tetrapyrrolic molecule.[2b,8d,e,h] The merit parameter, which characterizes molecular ability to initiate the PDT process, all other factors being equal, is a product of the 2PA cross section and quantum yield of singlet oxygen generation, $\sigma_2 \times \Phi_\Delta$. The measured Φ_Δ values are presented in Table 5 along with the merit factor at the wavelength of the maximum attainable σ_2 (which is not necessarily the 2PA spectral maximum in all cases). This Table also presents the wavelength of the linear fluorescence maximum.

TABLE 5: Singlet Oxygen Photosensitization Properties of the Studied Molecules

molecule	λ_{exc}^a (nm)	σ_2^b (GM)	Φ_Δ^c	$\sigma_2 \times \Phi_\Delta^d$ (GM)	$\lambda_{fl}(max)^e$ (nm)
yPy	833	20	1.1 ± 0.1	22	652
PyP	821	8200	0.84 ± 0.08	6900	730
PyyP	830	5500	0.84 ± 0.05	4600	711
yPyyPy	873	9100	0.54 ± 0.18	4900	756
yPyByPy	859	3800	1.1 ± 0.1	4200	697
yPyTyPy	871	3100	0.91 ± 0.09	2800	725
yPyAyPy	838	9000	0.3 ± 0.3	2700	770

[a] Best excitation wavelength for 2PA photosensitization of singlet oxygen. [b] 2PA cross section at this wavelength. [c] Quantum yield of singlet oxygen generation. [d] Figure of merit for two-photon sensitization of singlet oxygen. [e] Molecule fluorescence maximum.

$I = AP^b$,
$b = 2.2 +/- 0.3$
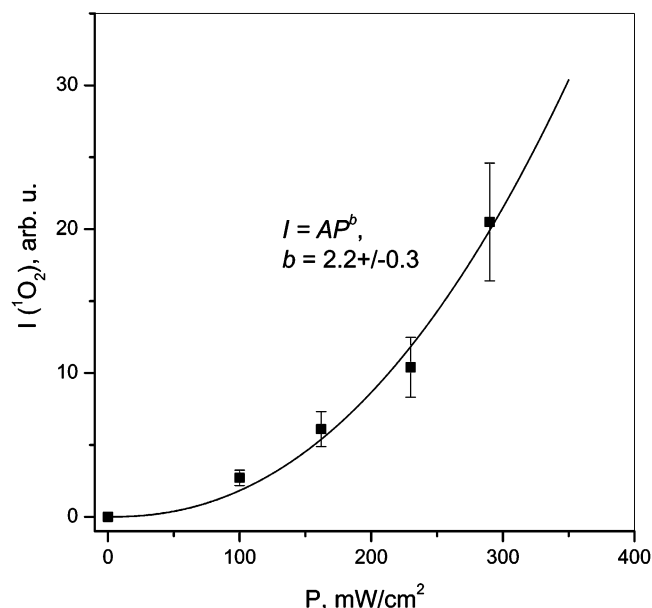
Figure 6. Dependence of the spectrally integrated luminescence intensity of singlet oxygen molecules around 1270 nm on average excitation power of Ti:sapphire amplifier laser, tuned to 807 nm, in toluene/1% pyridine solution of the PyP dimer. The power exponent of the best fitting function is close to 2, which confirms the 2PA mechanism of singlet oxygen photosensitization in this system.

First of all, we observe that Φ_Δ systematically decreases with the fluorescence maximum of the molecule shifting to the red. This effect is most probably explained by the energy conservation rule, which requires that the minimum possible triplet energy of a photosensitizer molecule must be higher than the triplet energy of oxygen. We will consider this result in more detail in a forthcoming publication.

Here we emphasize that the highest values of $\sigma_2 \times \Phi_\Delta$ are shown by PyP dimer (6900 GM) near to 820 nm and by yPyyPy dimer (4900 GM) near 870 nm. Note that the last wavelength is even more preferable in terms of better penetration through biological tissue, which could compensate for the slightly lower $\sigma_2 \times \Phi_\Delta$.

To demonstrate an ability to generate singlet oxygen via two-photon excitation, we have measured the dependence of singlet oxygen luminescence intensity on excitation power in a solution of the PyP dimer, using Ti:sapphire laser pulses at 807 nm. This dependence follows a quadratic law, as shown in Figure 6, thus proving that the molecule is indeed excited by simultaneous absorption of two near-IR photons.

Note that the dimers described in this article can also potentially be used in two-photon fluorescence microscopy, because their fluorescence quantum yields Φ_F vary between 0.05

Strong NIR 2PA in Conjugated Porphyrin Dimers

J. Phys. Chem. B, Vol. 109, No. 15, 2005 **7235**

and 0.1,[19] and therefore their two-photon excited fluorescence figures of merit are rather high, $\sigma_2 \times \Phi_F = 200-700$ GM (cf. refs 9, 13, and 14). Taking into account that the fluorescence occurs in the near-IR tissue "transparency window", this can make them unique markers for 3D biological imaging.

4. Conclusions

We have presented here the 2PA data for a series of conjugated porphyrin dimers and the corresponding monomer. All of the dimers show a pronounced 2PA peak at 820−890 nm, with very large cross section values, $\sigma_2 = (3-10) \times 10^3$ GM, which is several hundred times larger than that obtained for corresponding monomer. We explain such dramatic cooperative enhancement by a combination of several factors, including strong enhancement of the lowest one-photon Q-transition, better resonance conditions in the three-level system, dramatic enhancement of the excited-state singlet−singlet transition due to linear elongation of the π-conjugated system, and parallel arrangement of consecutive transitions in dimers, as compared to the perpendicular one in the monomer. We show that the absolute values of the 2PA cross sections in these molecules are quantitatively described by a quantum-mechanical expression, derived for the three-level model. We also demonstrate the possibility of singlet oxygen generation upon one- and two-photon excitation of these dimers, which make them particularly attractive for PDT.

References and Notes

(1) (a) Zipfel, W. R.; Williams, R. M.; Webb, W. W. *Nat. Biotechnol.* **2003**, *21*, 1369, and references therein. (b) Blanchard-Desce, M.; *C. R. Acad. Sci. Ser. IV: Phys. Astrophys.* **2002**, *3*, 439, and references therein.

(2) (a) Bhawalkar, J. D.; Kumar, N. D.; Zhao, C.-F.; Prasad, P. N. *J. Clin. Lasers Med. Surg.* **1997**, *15*, 201. (b) Karotki, A.; Kruk, M.; Drobizhev, M.; Rebane, A.; Nickel, E.; Spangler, C. W. *IEEE J. Sel. Top. Quantum Electron.* **2001**, *7*, 971.

(3) (a) Cumpston, B. H.; Ananthavel, S. P.; Barlow, S.; Dyer, D. L.; Ehrlich, J. E.; Erskine, L. L.; Heikal, A. A.; Kuebler, S. M.; Lee, I.-Y. S.; McCord-Maughon, D.; Qin, J.; Röckel, H.; Rumi, M.; Wu, X.-L.; Marder, S. R.; Perry, J. W. *Nature* **1999**, *398*, 51. (b) Zhou, W.; Kuebler, S. M.; Braun, K. L.; Yu, T.; Cammack, J. K.; Ober, C. K.; Perry, J. W.; Marder, S. R. *Science* **2002**, *296*, 1106.

(4) (a) Parthenopoulos, D. A.; Rentzepis, P. M. *Science* **1989**, *245*, 843. (b) Burr, G. W. Volumetric Storage. In *Encyclopedia of Optical Engineering*; Driggers, R. G., Ed.; Marcel Dekker: New York, 2003, and references therein.

(5) (a) Bonnett, R. *Chem. Soc. Rev.* **1995**, *24*, 19, and references therein. (b) Prasad, P. N. *Introduction to Biophotonics*; Wiley-Interscience: Hoboken, NJ, 2003; Chapter 12, and references therein.

(6) Renn, A.; Wild, U. P.; Rebane, A. *J. Phys. Chem. A* **2002**, *106*, 3045.

(7) (a) Vsevolodov, N. N.; Kostikov, L. P.; Kayushin, L. P.; Gorbatenkov, V. I. *Biophysics* **1973**, *18*, 755. (b) Meshalkin, Yu. P.; Alfimov, E. E.; Vasil′ev, N. E.; Denisov, A. N.; Makukha, V. K.; Ogirenko, A. P. *Quantum Electron.* **1999**, *29*, 1066. (c) Goyan, R. L.; Cramb, D. T. *Photochem. Photobiol.* **2000**, *72*, 821.

(8) (a) Drobizhev, M.; Karotki, A.; Rebane, A. *Chem. Phys. Lett.* **2001**, *334*, 76. (b) Karotki, A.; Kruk, M.; Drobizhev, M.; Rebane, A. *J. Mod. Opt.* **2002**, *49*, 379. (c) Drobizhev, M.; Karotki, A.; Kruk, M.; Rebane, A. *Chem. Phys. Lett.* **2002**, *355*, 175. (d) Drobizhev, M.; Karotki, A.; Kruk, M.; Mamardashvili, N. Zh.; Rebane, A. *Chem. Phys. Lett.* **2002**, *361*, 504. (e) Karotki, A.; Drobizhev, M.; Kruk, M.; Spangler, C.; Nickel, E.; Mamardashvili, N.; Rebane, A. *J. Opt. Soc. Am. B*, **2003**, *20*, 321. (f) Drobizhev, M.; Karotki, A.; Kruk, M.; Krivokapic, A.; Anderson, H. L.; Rebane, A. *Chem. Phys. Lett.* **2003**, *370*, 690. (g) Karotki, A.; Drobizhev, M.; Dzenis, Y.; Taylor, P. N.; Anderson, H. L.; Rebane, A. *Phys. Chem. Chem. Phys.* **2004**, *6*, 7. (h) Drobizhev, M.; Karotki, A.; Kruk, M.; Dzenis, Y.; Rebane, A.; Meng, F.; Nickel, E.; Spangler, C. W. *Proc. SPIE−Int. Soc. Opt. Eng.* **2003**, *5211*, 63.

(9) (a) Albota, M.; Beljonne, D.; Brédas, J.-L.; Ehrlich, J. E.; Fu, J.-Y.; Heikal, A. A.; Hess, S. E.; Kogej, T.; Levin, M. D.; Marder, S. R.; McCord-Maughon, D.; Perry, J. W.; Röckel, H.; Rumi, M.; Subramaniam, G.; Webb, W. W.; Wu, X.-L.; Xu, C. *Science* **1998**, *281*, 1653. (b) Drobizhev, M.; Karotki; A.; Rebane, A.; Spangler, C. W. *Opt. Lett.* **2001**, *26*, 1081.

(10) Ogawa, K.; Ohashi, A.; Kobuke, Y.; Kamada, K.; Ohta, K. *J. Am. Chem. Soc.* 2003, *125* 13356.

(11) Screen, T. E. O.; Thorne, J. R. G.; Denning, R. G.; Bucknall, D. G.; Anderson, H. L. *J. Am. Chem. Soc*., **2002**, *124*, 9712.

(12) A brief communication on some aspects of the work detailed here was presented in Drobizhev, M.; Stepanenko, Y.; Dzenis, Y.; Karotki, A.; Rebane, A.; Taylor, P. N.; Anderson, H. L. *J. Am. Chem. Soc.* **2004**, *126*, 15352.

(13) Xu, C.; Webb, W. W. *J. Opt. Soc. Am. B* **1996**, *13*, 481.

(14) Rumi, M.; Ehrlich, J. E.; Heikal, A. A.; Perry, J. W.; Barlow, S.; Hu, Z.; McCord-Maughon, D.; Parker, T. C.; Röckel, H.; Thayumanavan, S.; Marder, S. R.; Beljonne, D.; Brédas, J.-L. *J. Am. Chem. Soc.* **2000**, *122*, 9500.

(15) Galanin, M. D.; Chizhikova, Z. A. *JETP Lett.* **1966**, *4*, 27.

(16) Lakowicz, J. R. *Principles of Fluorescence Spectroscopy*; Plenum Press: New York, 1983; Chapter 5.

(17) Ganzha, V. A.; Gurinovich, G. P.; Dzhagarov, B. M.; Egorova, G. D.; Sagun, E. I.; Shul′ga, A. M. *J. Appl. Spectrosc.* **1989**, *50*, 402.

(18) Lin, V. S.-Y.; DiMagno, S. G.; Therien, M. J. *Science* **1994**, *264*, 1105.

(19) Taylor, P. N.; Wylie, A. P.; Huuskonen, J.; Anderson, H. L., *Angew. Chem., Int. Ed.* **1998**, *37*, 986.

(20) (a) Anderson, H. L. *Tetrahedron Lett.* **1992**, *33*, 1101. (b) Anderson, H. L.; Martin, S. J.; Bradley, D. D. C. *Angew. Chem., Int. Ed. Engl.* **1994**, *33* 655.

(21) Beljonne, D.; O'Keefe, G. E.; Hamer, P. J.; Friend, R. H.; Anderson, H. L.; Brédas, J.-L. *J. Chem. Phys.* **1997**, *106*, 9439.

(22) Shediac, R.; Gray, M. H. B.; Uyeda, H. T.; Johnson, R. C.; Hupp, J. T.; Angiolillo, P. J.; Therien, M. J. *J. Am. Chem. Soc.* **2000**, *122*, 7017.

(23) Piet, J. J.; Taylor, P. N.; Anderson, H. L.; Osuka, A.; Warman, J. M. *J. Am. Chem. Soc.* **2000**, *122*, 1749.

(24) Gouterman, M. *J. Chem. Phys.* **1959**, *30*, 1139.

(25) Anderson, H. L. *Adv. Mater.* **1994**, *6*, 834.

(26) (a) O'Keefe, G. E.; Denton, G. J.; Harvey, E. H.; Phillips, R. T.; Friend, R. H.; Anderson, H. L. *J. Chem. Phys.* **1996**, *104*, 805. (b) Taylor, P. N.; Huuskonen, J.; Rumbles, G.; Aplin, R. T.; Williams, E.; Anderson, H. L. *Chem. Commun.* **1998**, 909.

(27) Kuz′mitskii, V. A.; Solov′ev, K. N. *J. Appl. Spectrosc.* **1983**, *38*, 217.

(28) (a) Stranger, R.; McGrady, J. E.; Arnold, D. P.; Lane, I.; Heath, G. A. *Inorg. Chem.* **1996**, *35*, 7791. In this paper, the long molecular axis in the dimer was designated as the *y*-axis and the short one as the *x*-axis; see comment in (b) Arnold, D. P.; Heath, G. A.; James, D. A. *J. Porphyrins Phthalocyanines* **1999**, *3*, 5.

(29) Jeong, D. H.; Jang, S. M.; Hwang, I.-W.; Kim, D.; Yoshida, N.; Osuka, A. *J. Phys. Chem. A* **2002**, *106*, 11054.

(30) (a) Bayliss, N. S. *J. Chem. Phys.* **1948**, *16*, 287. (b) Kuhn, H. *J. Chem. Phys.* **1949**, *17*, 1198.

(31) Arnold, D. P. Private communication.

(32) Zhou, X.; Ren, A.-M.; Feng, J.-K.; Liu, X.-J.; Zhang, Y.-D. *ChemPhysChem* **2003**, *4*, 991.

(33) Rubtsov, I. V.; Susumu, K.; Rubtsov, G. I.; Therien, M. J. *J. Am. Chem. Soc.* **2003**, *125*, 2687.

(34) Arnold, D. P.; James, D. A.; Kennard, C. H. L.; Smith, G. *J. Chem. Soc., Chem. Commun.* **1994**, 2131.

(35) Kumble, R.; Palese, S.; Lin, V. S.-Y.; Therien, M. J.; Hochstrasser, R. M. *J. Am. Chem. Soc.* **1998**, *120*, 11489.

(36) (a) Masthay, M. B.; Findsen, L. A.; Pierce, B. M.; Bocian, D. F.; Lindsay, J. S.; Birge, R. R. *J. Chem. Phys.* **1986**, *84*, 3901. (b) Birge, R. R. *Acc. Chem. Res.* **1986**, *19*, 138.

(37) Boyd, R. W. *Nonlinear Optics*, 2nd ed.; Academic Press: Amsterdam, 2003; Chapter 12.

(38) Meath, W. J.; Power, E. A. *J. Phys. B: At., Mol. Opt. Phys.* **1984**, *17*, 763.

(39) Atkins, P. W.; Friedman, R. S. *Molecular Quantum Mechanics*, 3rd ed.; Oxford University Press: Oxford, 1997.

(40) In a five-level system, we only have to substitute $|\mu_{fi}|^2/h\nu_{fi}$ with $|\mu_{fi}|^2/h\nu_{fi} + |\mu_{ei}|^2/h\nu_{ei}$ in eqs 11 and 12 and consider an additional equation for the experimentally measured ratio of the blue and red peak areas, $A_{blue}/A_{red} = |\mu_{fi}|^2/\nu_{fi}|/|\mu_{fe}|^2/\nu_{fe}^2$, where the index e corresponds to the "red" 2PA state.

(41) Karafiloglou, P.; Launay, J.-P. *Chem. Phys.* **2003**, *289*, 231.

(42) (a) Heflin, J. R.; Wong, K. Y.; Zamani-Khamiri, O.; Garito, A. F. *Phys. Rev. B* **1988**, *38*, 1573. (b) Wu, J. W.; Heflin, J. R.; Norwood, R. A.; Wong, K. Y.; Zamani-Khamiri, O.; Garito, A. F.; Kalyanaraman, P.; Sounik, J. *J. Opt. Soc. Am. B* **1989**, *6*, 707. (c) Soos, Z. G.; Ramasesha, S. *J. Chem.*

Drobizhev et al.

Phys. **1989**, *90*, 1067. (d) Dixit, S. N.; Guo, D.; Mazumdar, S. *Phys. Rev.* **1991**, *43*, 6781. (e) McWilliams, P. C. M.; Hayden, G. W.; Soos, Z. G. *Phys. Rev. B* **1991**, *43*, 9777. (f) Shuai, Z.; Beljonne, D.; Brédas, J. L. *J. Chem. Phys.* **1992**, *97*, 1132. (g) Mazumdar, S.; Guo, D.; Dixit, S. N. *J. Chem. Phys.* **1992**, *96*, 6862. (h) Abe, S.; Schreiber, M.; Su, W. P.; Yu, J. *Phys. Rev. B* **1992**, *45*, 9432. (i) Luo, Y.; Ågren, H.; Stafström, S. *J. Phys. Chem.* **1994**, *98*, 7782. (j) Chandross, M.; Shimoi, Y.; Mazumdar, S. *Chem. Phys. Lett.* **1997**, *280*, 85. (k) Norman, P.; Luo, Y.; ; Ågren, H. *Chem.*

Phys. Lett. **1998**, *296*, 8. (l) Norman, P.; Luo, Y.; Ågren, H. *Opt. Commun.* **1999**, *168*, 297. (m) Chandross, M.; Shimoi, Y.; Mazumdar, S. *Phys. Rev. B* **1999**, *59*, 4822. (n) Race, A.; Barford, W.; Bursill, R. J. *Phys. Rev. B* **2001**, *64*, 035208.

(43) Rashba, E. I.; Gurgenishvili, G. E. *Sov. Phys. Solid State* **1962**, *4*, 759.

(44) Thorne, J. R. G.; Kuebler, S. M.; Denning, R. G.; Blake, I. M.; Taylor, P. N.; Anderson, H. L. *Chem. Phys.* **1999**, *248*, 181.